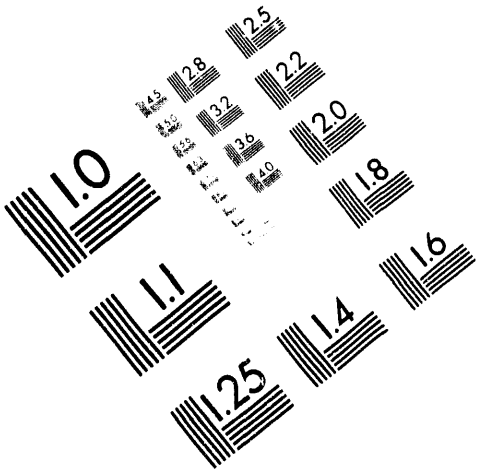

Association for Information and Image Management

1100 Wayne Avenue, Suite 1100
Silver Spring, Maryland 20910

301/587-8202

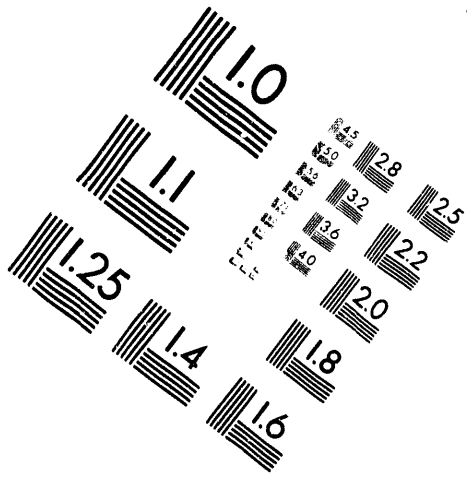

Centimeter

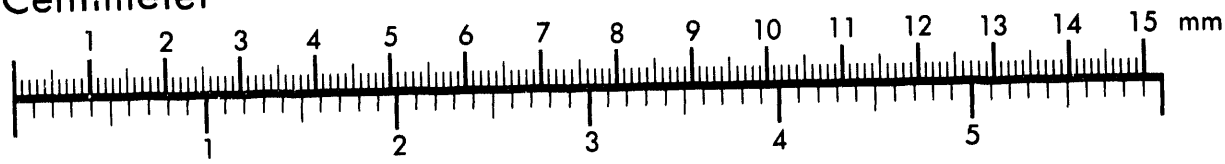

Inches

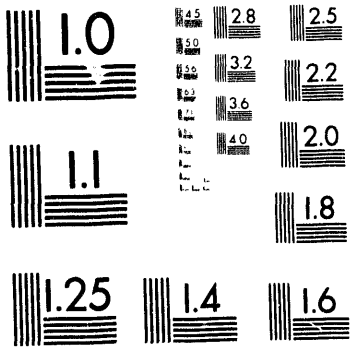

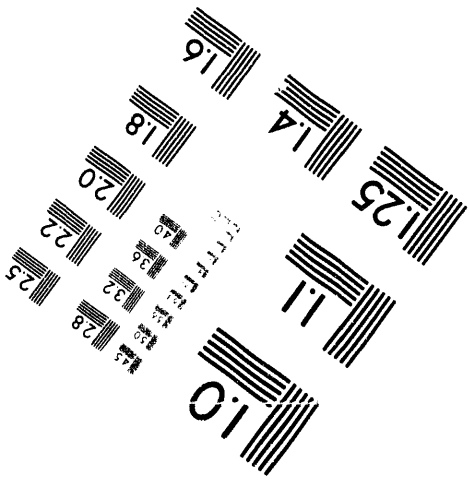

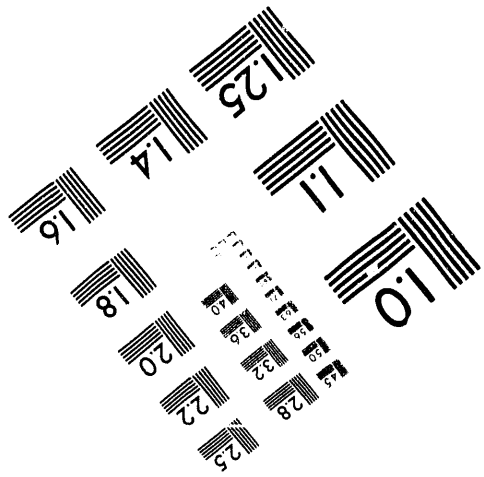

MANUFACTURED TO AIIM STANDARDS
BY APPLIED IMAGE, INC.

1 of 1

Conf-9301119--1

UCRL-JC-112686
PREPRINT

RECEIVED
JUL 19 1993
OSTI

Dynamics of Short-Pulse Excitation, Ionization and Harmonic Conversion

K. C. Kulander, K. J. Schafer, and J. L Krause

This paper was prepared for submittal to the
NATO Workshop
Han-Sur-Lesse, Belgium
January 8–14, 1993

January 1993

Lawrence Livermore National Laboratory

This is a preprint of a paper intended for publication in a journal or proceedings. Since changes may be made before publication, this preprint is made available with the understanding that it will not be cited or reproduced without the permission of the author.

MASTER

DISTRIBUTION OF THIS DOCUMENT IS UNLIMITED

DISCLAIMER

This document was prepared as an account of work sponsored by an agency of the United States Government. Neither the United States Government nor the University of California nor any of their employees, makes any warranty, express or implied, or assumes any legal liability or responsibility for the accuracy, completeness, or usefulness of any information, apparatus, product, or process disclosed, or represents that its use would not infringe privately owned rights. Reference herein to any specific commercial product, process, or service by trade name, trademark, manufacturer, or otherwise, does not necessarily constitute or imply its endorsement, recommendation, or favoring by the United States Government or the University of California. The views and opinions of authors expressed herein do not necessarily state or reflect those of the United States Government or the University of California, and shall not be used for advertising or product endorsement purposes.

DYNAMICS OF SHORT-PULSE EXCITATION, IONIZATION AND HARMONIC CONVERSION

K. C. Kulander, K. J. Schafer and J. L. Krause*

Physics Department
Lawrence Livermore National Laboratory
Livermore, CA 94551

INTRODUCTION

In recent years there have been very significant advances in short pulse, high intensity laser technology. Lasers with pulse lengths of 0.1-1 ps and wavelengths from 0.2-1 μm can be focused to produce intensities from 10^{12} to above 10^{18} W/cm^2. One major use of these systems has been for studies of the response of atoms and molecules to such intense, well characterized electromagnetic fields. Because these pulses are very short, neutral atoms can survive to experience intensities where theoretical treatments based on the traditional perturbation expansion of the wave function in terms of the field-free states will fail completely to describe the dynamics of the system. An explicit, non-perturbative time-dependent calculation is one approach which can represent these strong field effects.

Evidence for non-perturbative ionization can be found, for example, in the photoelectron energy spectra which contain numerous peaks separated by the photon energy. This spectrum demonstrates a high probability for the absorption of *many* more photons than the minimum required for ionization. This phenomenon, called above threshold ionization (ATI), has been observed in several experiments[1] and can be obtained theoretically from an energy analysis of the final state wave function obtained from a time-dependent calculation.[2] A second remarkable observation in high intensity experiments is the efficient production of *very* high-order harmonic radiation during the laser pulse. In the direction of propagation of the incident beam, strong coherent emission at odd multiples of the driving frequency is produced. The even harmonics are forbidden by symmetry. Harmonics up to the 109th order of a 140 fs Ti-sapphire (806 nm) laser[3a] and 133rd harmonic of a 1053 nm 1 ps Nd-YLF laser[3b] have been obtained in neon. Again, the time-dependent wave function contains the information that explains this highly nonlinear, non-perturbative behavior. The Fourier

transform of the dipole induced in the electronic charge distribution gives the spectrum of emitted radiation. For many atomic systems, the spectra calculated using this technique agree quantitatively with the observed harmonic emission.[4]

In this paper we discuss recent calculations for xenon in pulsed laser fields which illustrate the multiphoton processes described above. In these calculations we have employed a single-active-electron (SAE) model which explicitly follows the separate time evolution of each of the valence electrons in the frozen, mean-field of the remaining, unexcited electrons, the nucleus and the laser field. This model works well for the rare gas atoms, at least partially because the neglected double or higher excitations involve states well above the ionization threshold. In the next section we give a brief description of the SAE model, emphasizing in particular the development of ion-core specific effective potentials. We present ionization, photoelectron and photoemission rates for xenon at 1.06 μm and compare them to recent experimental results in the third section. We show that harmonics and ATI although related are not identical. The electron energy distributions do not show the cutoff observed in harmonics. After describing the quantum mechanical results and comparing them to recent experiments, we will present a simple two-step, quasi-classical model which explains these differences and which gives a more complete understanding of the dynamics of non-perturbative excitation.

METHOD AND MODEL

A many electron atom in an intense, pulsed laser field is a formidable computational problem. This is because the Hamiltonian,

$$H(t) = H_o + V_l(t), \tag{1}$$

is explicitly time dependent. H_0 is the (non-relativistic) atomic Hamiltonian and $V_l(t)$ is the interaction between the electron and the field. In many of the short-pulse experiments carried out today, V_l is comparable in strength to the Coulombic interactions within the atom. Therefore the method of solution must be able to treat these different interactions on an equal footing. Because the full multielectron problem is beyond present computational capabilities, we have developed a model based on the Hartree-Fock method in which the time-dependent wave function in approximated by a product of single particle orbitals. This approach can provide considerable insight into the excitation dynamics as well as quantitative predictions for the observed multiphoton processes.

The laser is assumed to be linearly polarized along the z-axis and the field is strong enough to be treated semiclassically. Then

$$V_l(t) = -e\sum_i z_i \mathcal{E}_o f(t)\sin(\omega t). \tag{2}$$

Here ε_0 is the magnitude of the field and ω is the frequency. The pulse envelope $f(t)$ is typically chosen to be either a sine-squared or trapezoidal pulse. If we are interested in calculating quantities relevant to a particular intensity, $I_0 = c\varepsilon_0^2/8\pi$, we choose a pulse envelope that rises over several optical cycles to its maximum value (1.0) and then is held constant for 20-30 cycles. The pulse rise must involve at least a few cycles or the calculated results can be contaminated by unphysical transients.

The calculations reported here have been performed using the SAE approximation. The details of these calculations have been presented elsewhere[5] and will be repeated here only to the extent necessary to describe a recent improvement we have made in the effective potentials. In this model we hold the orbitals of all but one of the electrons in the atom fixed and allow the active electron to respond to the laser in the mean field of the remaining electrons and the nucleus.

The effective potentials for the active electron are generated according to the prescription given previously.[6] The potentials are constructed from valence orbitals of the atom obtained from Hartree-Slater calculations for the ground and singly-excited states of the atom. The exchange-correlation parameter is adjusted so that the orbital energy of interest agrees with the spectroscopic value. The valence orbital, which has a particular value of the orbital angular momentum, ℓ, is then used to construct an ℓ-dependent effective potential whose lowest eigenvalue is the ionization energy of that state. A separate calculation is carried out for each ℓ-value to generate the complete potential. We use the $\ell = 2$ potential for $\ell \geq 2$. This results in quite accurate excitation energies, much better than normally obtained in either Hartree-Fock or Hartree-Slater calculations. This procedure will provide a model of xenon which accounts only for the manifold of singly excited states based on the lowest ionic core, $^2P_{3/2}$. For all rare gases, a second manifold of states converges to the next spin-orbit component of the ion, the $^2P_{1/2}$ state. Therefore, we repeat the above procedure to obtain effective potentials for this second set of excited states. We further assume that multiphoton excitations between these two manifolds are very weakly coupled on the time scale of the multiphoton processes of interest so they can be treated separately. This assumption is reasonable because once one of the electrons is excited outside a particular core configuration, transitions into states with the other core requires two electrons to change state. Thus it is within the spirit of the SAE approximation to neglect such excitation pathways. However, in calculating the induced dipole responsible for the harmonic emission we add coherently the contributions from the separate calculations for the two manifolds.

We have constructed such core-specific effective potentials for all the rare gases. In xenon the splitting between the ion core limits is quite large, approximately 1.3 eV. Therefore the contributions from its second manifold are significant only in photoemission for the range of intensities and wavelengths considered here. However, for very short laser pulses, the atom can experience higher laser intensities and the contributions from these states will become relatively more important. We have found that for all the lighter rare gases,

including krypton where the ionic cores are separated by 0.66 eV, the additional manifold of excited states is very important, and for some wavelengths and intensities, can be dominant.[7,8]

Another important effect due to the spin-orbit coupling comes into play whether the upper ionic core is specifically involved or not. This is because the excitation dynamics is very sensitive not only to the ionization potential or binding energy of the active electron but also to m, the projection of the orbital angular momentum along the polarization axis. Since no spin-orbit terms are explicitly included in our Hamiltonian, we solve the Schrödinger equation in LS-coupling. This means that for a linearly polarized laser field, m is a good quantum number. Therefore, we need to assign weights to the valence orbitals according to their weights in the spin-orbit coupled states. In earlier calculations on xenon, the valence shell p-electrons with $m = 0$ were found to provide the dominant contribution to the ionization[9] and photoemission[10] rates. There are two $m = 0$ valence electrons in the p-shell, 4/3 associated with the $^2P_{3/2}$ core and 2/3 with $^2P_{1/2}$. Contributions to the ionization rates and harmonic emission strengths from the other four p-electrons in the valence shell of krypton which have $m = \pm 1$ are found to be unimportant for the intensities considered here. Thus we solve the time-dependent Schrödinger equation,

$$i\hbar \frac{\partial}{\partial t} \psi_j(t) = H_j(t) \psi_j(t) \tag{3}$$

for the 4/3 electrons with $m = 0$ that leave the ion in the $^2P_{3/2}$ state and the 2/3 electrons with $m = 0$ that leave the ion in the $^2P_{1/2}$ state. In Eq. (3), $\psi_j(t)$ is the active-electron orbital which at $t = 0$ is the valence pseudo-orbital with total angular momentum j, and H_j contains the appropriate effective potentials. Ionization and photoemission rates are determined during the last part of the pulse which rises to its maximum intensity over five optical cycles and then has a constant intensity for the next 20-30 cycles. After the ramp, the transient excitations decay by ionization over the next few cycles. We obtain an ionization rate by monitoring the norm of the wave function. Our finite difference integration of Eq. (3) is carried out in a finite box with absorbing boundaries. As flux reaches the edges of the grid it is removed. The rate at which this occurs is defined to be the ionization rate.

The emission strengths at the harmonic frequencies are proportional to the square of the Fourier transform of the total induced dipole, which we typically calculate over the last five cycles of the pulse described above:

$$d_q = \frac{1}{T_f - T_i} \sum_j \int_{T_i}^{T_f} dt\, e^{-iq\omega t} \langle \psi_j(t) | z | \psi_j(t) \rangle . \tag{4}$$

In fact we have found it better to use the acceleration form of the dipole, which is numerically more tractable, for determining the time-dependent dipole.[11,12] For energy and angular

distributions of the ejected electrons, we choose a pulse which also turns off over a few additional cycles (a trapezoidal pulse) and then perform an analysis of the final wave function using an energy window function.[2]

RESULTS

In this section we illustrate the methods we have defined above by considering the response of a xenon atom to an intense 1.06 μm laser field. We present electron and photon emission rates for laser intensities well into the non-perturbative regime, above 10^{13} W/cm^2. In particular, we will show that although the harmonics and ATI are related they are not identical. We then present a simple two-step, quasi-classical model which addresses these differences.

Ionization and Photoelectron Emission from Xenon

We have studied the excitation of xenon by 1.06 μm radiation for intensities between 5×10^{12} and 5×10^{13} W/cm^2. In Fig. 1 we show the measured[13] ion yields for the first three ion charge states as functions of intensity for a 50 ps pulse. The calculated yield for Xe^{+1} is

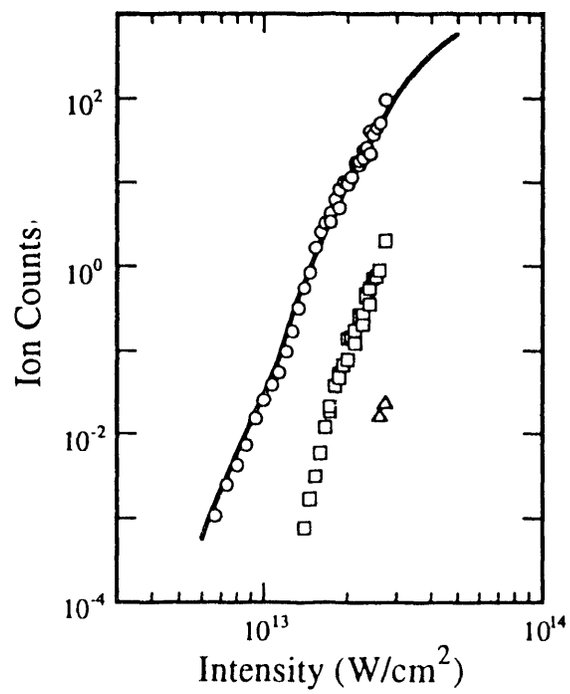

Fig. 1 Calculated (line) and measured (symbols) xenon ion yields as functions of intensity: Xe^{+1} (circles), Xe^{+2} (squares) and Xe^{+3} (triangles).

given by the solid line. Here some small shift of the reported experimental intensity (much less than the maximum expected uncertainty of 50 per cent) has been made to obtain the agreement shown. Having calibrated our results against ion yield curves, we can then compare our electron or photon emission strengths in a consistent manner. The calculated ion yield curve has been averaged over the temporal and spatial distributions in the focal volume. In Fig. 2 we show the ATI spectra for intensities below saturation both calculated (single-atom) and measured. Because of uncertainties in detector efficiency the vertical scale for the experimental data has been shifted so the the two spectra agreed for the 24th order peak at the intermediate intensity.

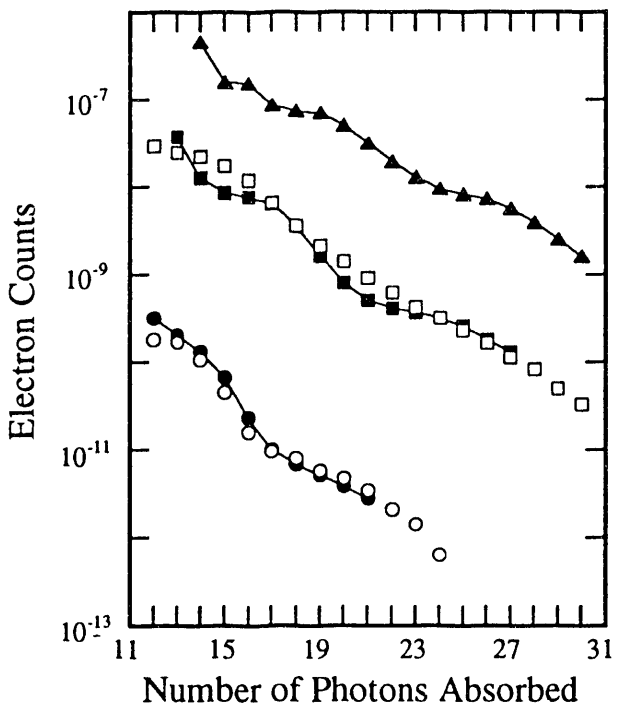

Fig. 2 Photoelectron kinetic energy (ATI) spectrum for Xe at 1.05 μm at 1 (circles), 1.5 (squares) and 2 (triangles) x10^{13} W/cm^2: Calculated (filled symbols), Measured (open symbols).

Finally, we complete our presentation of the predicted and observed emission rates for xenon by showing the intensity dependence of the harmonic yields for a 36 ps YAG laser. In Fig 3 we show an absolute comparison[14] between the calculated and measured number of harmonic photons as functions of order for four different incident intensities. One can see that as the intensity increases the spectrum develops an increasingly broad plateau of harmonics which have approximately equal strength and then an abrupt cutoff. The calculated spectra include the macroscopic effects of propagation through the excited, and ionized, medium within the focal volume. Although these propagation effects can affect the overall strength of the emission, the spectral shape observed is very similar to the single-atom

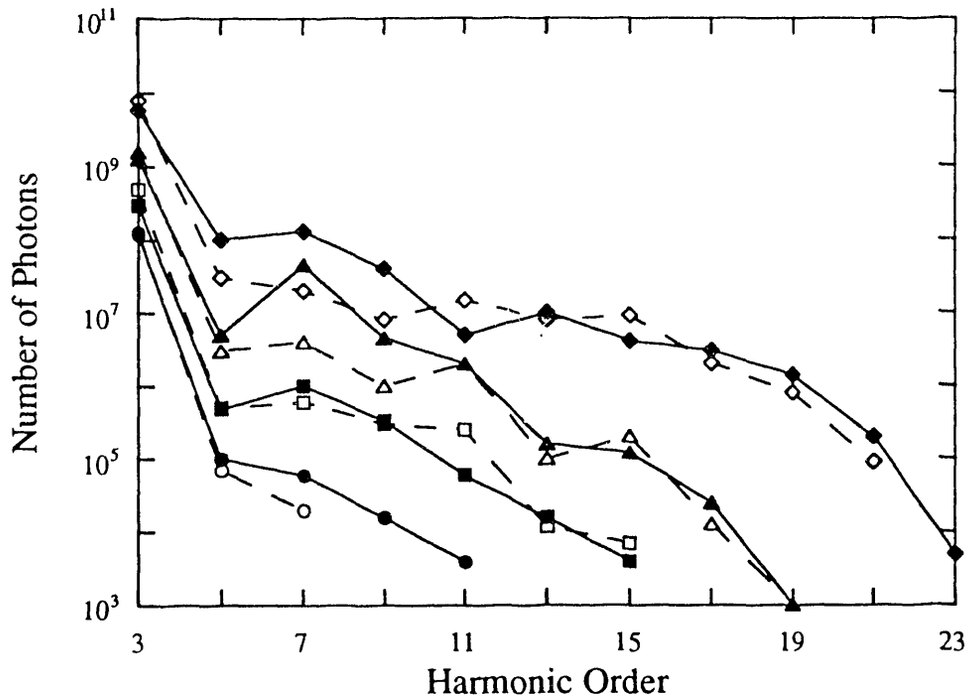

Fig. 3 Harmonic photon yields for Xe at 1.06 μm at 1 (circles), 1.3 (squares), 2 (triangles) and 4 (diamonds) x10^{13} W/cm^2: Calculated (filled symbols), Measured (open symbols).

emission strengths. In the high intensity regime phase matching of the harmonics within the plateau is almost order-independent.[4,15]

Two-step quasiclassical model for high field ionization

In the high intensity regime we find that a new contribution to harmonic emission becomes possible. At lower intensities the familiar nonlinear susceptibilities which exist because of the anharmonicity of the atomic potential result from relatively small displacements of the electronic charge density. The intensity dependences of these components of the overall induced polarization are provided by perturbation theory. Thus the q-th order susceptibility scales as the q-th power of the driving field. We show in Fig. 4a a schematic "perturbative" harmonic spectrum for two intensities which differ by a factor of 2. At higher intensities a new source of high energy photoemission becomes probable. In a strong, low frequency field electrons can escape from the vicinity of the ion core by tunnelling through the barrier formed by the Coulomb attraction of the core and the instantaneous electric field due to the laser. This barrier is narrowest along the axis of polarization, so that electrons will be released near this axis, approximately at the point on the outer edge of the barrier where the binding energy is equal to the initial state's ionization

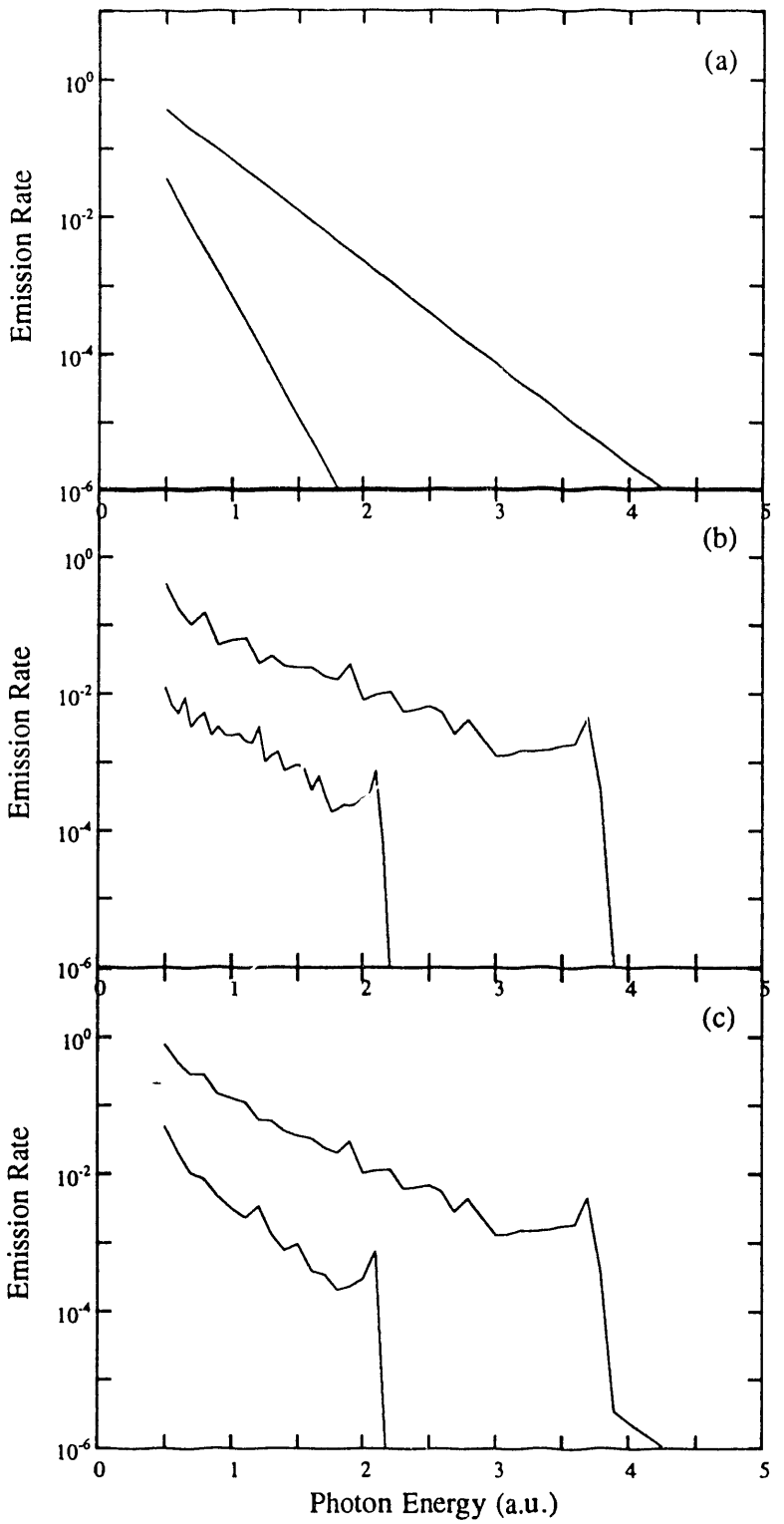

Fig. 4 (a) Schematic perturbative harmonic emission strengths. (b) Quasi-classical emission strengths from trajectory calculations. (c) Sum of two contributions. In all three cases intensity for the upper curve is twice that for the lower.

potential. We show a cut of the combined potentials for a particular electric field strength and the position, z_{init}, of the newly released electron in Fig. 5.

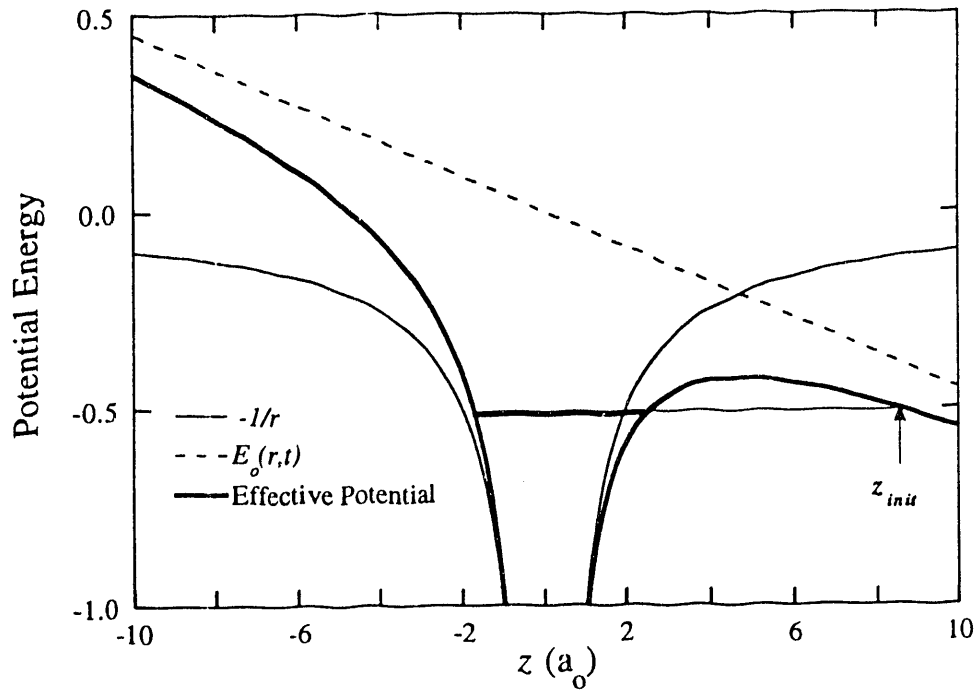

Fig. 5 Instantaneous effective potential for hydrogen in a field polarized along the z-axis. The ground state wave function (indicated by bold line within well) can ionize by tunnelling through the suppressed barrier. Electrons are released at z_{init}.

Tunnelling is most probable when the field is at its maximum ($\omega t=(n+1/2)\pi$ in Eq. (2)) which occurs twice during each optical cycle. Because the amplitude of the field varies slowly with the phase, there will be a finite interval around these maxima during which electrons will be freed. Using a simple tunnelling formula[16] we find the interval increases as the intensity increases. The relevance of this process to photon emission is that most of the electrons which escape through the barrier will be driven by the laser field back across the ion core at which time they may emit a photon. While the electron is near the nucleus it can make a transition back to the ground state, emitting a high energy photon. Obviously the energy of the resulting photon will correspond to the energy the electron has when it returns to vicinity of the core. This return energy depends strongly on the particular phase during the optical cycle at which the electron escaped through the barrier.

After tunnelling the density of states available to the electron is large enough that its subsequent evolution should be accurately characterized by classical mechanics. Therefore in the high intensity regime we can employ a two-step quasi-classical model to represent the ionization dynamics. The first step is the tunnelling process which frees some well defined fraction of the total electron wave function at each instant during the cycle. The second step is the classical motion of the electrons born outside the barrier. In Fig. 6 we show a phase space plot of a representative trajectory which was released with a phase which results in

multiple returns to the nucleus. The initial conditions of the trajectory were defined by zero velocity and the displacement along the direction of polarization corresponding to the outer point on the barrier produced by the field at that phase of the cycle. The potential used in the calculation is hydrogenic (soft-Coulomb[17]). The wavelength (1.82 μm) and intensity (1×10^{14} W/cm^2) were chosen to be well into the tunnelling regime. The amplitude of quiver motion of a free electron in this field is 84 a_0. The figure shows that the electron mostly moves as a free electron, occasionally experiencing abrupt collisions with the nucleus. Only when the electron is close to the nucleus can it release its energy by emitting a photon. We keep track of the energies at the return points and identify these as possible harmonic photons. Symmetry and the conservation of energy will require the photon frequency be an odd integral multiple of the driving frequency. The emission is dominated by transitions back to the ground state.

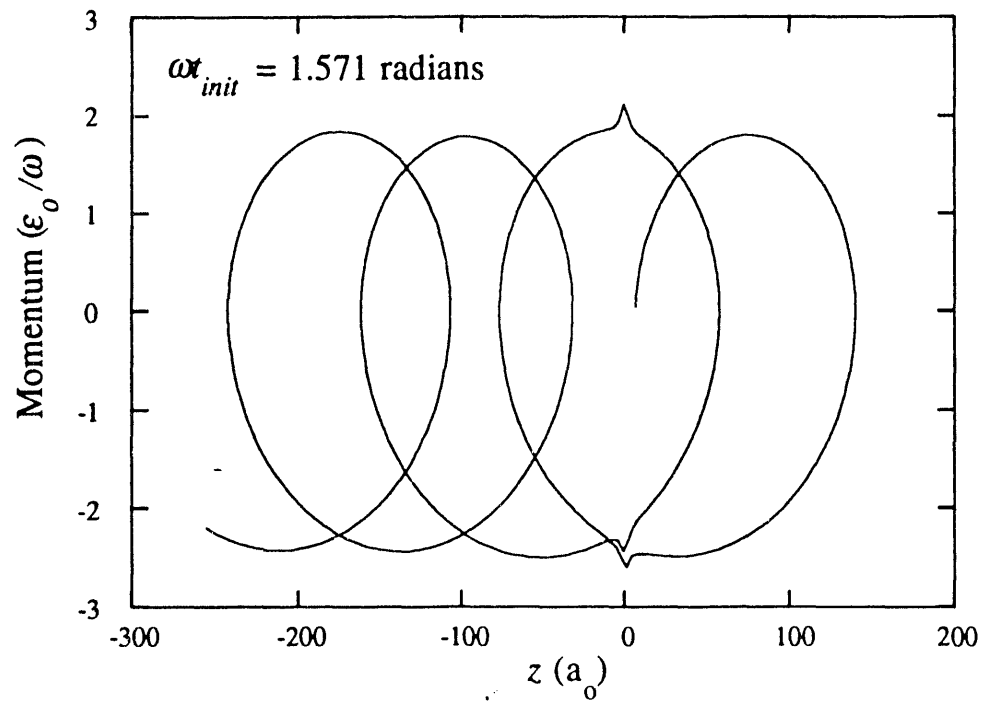

Fig. 6 Trajectory of an electron which tunnelled to freedom just before the maximum in the oscillating electric field.

We repeat the above procedure for each phase of the optical cycle and record the return energies of the electrons. We show in Fig. 7 the distribution of return energies obtained for 180 trajectories equally spaced in time over the first half of the cycle. The results are identical to that obtained during the second half by symmetry. The trajectories are followed for four cycles of the field. We plot the return energy in excess of the field-free binding energy in units of U_p, the ponderomotive (or quiver) energy of a free electron in the oscillating field. U_p is given by $I/4\omega^2$ in atomic units. We have also plotted the tunnelling

rate for hydrogen in this field as a function of the phase. A small fraction of the emitted electrons (about 25 percent in this case) initiated in the interval just after the phase $\pi/4$ drift away from the nucleus without a collision. Phases earlier than $\pi/4$ produce trajectories which do not recross the nucleus, but the tunnelling barrier is too broad for any significant release to occur. The rest of the trajectories return at least once. We see that for initial conditions near the maximum of the field the electron can undergo multiple collisions with the nucleus. This is because these initial conditions give the minimum in the initial drift velocity of the released electron. It is the drift velocity which is measured in ATI experiments, either directly in short pulse experiments or indirectly in long pulses due to the additional acceleration of the electron by the gradient of the focussed laser field. In the absence of collisions the maximum possible electron energy in long pulse experiments is $3U_p$. Electrons born with high drift energy generally will have at most one collision the nucleus. Because of this rescattering the final energy of the detected electron can be much larger than $3U_p$.

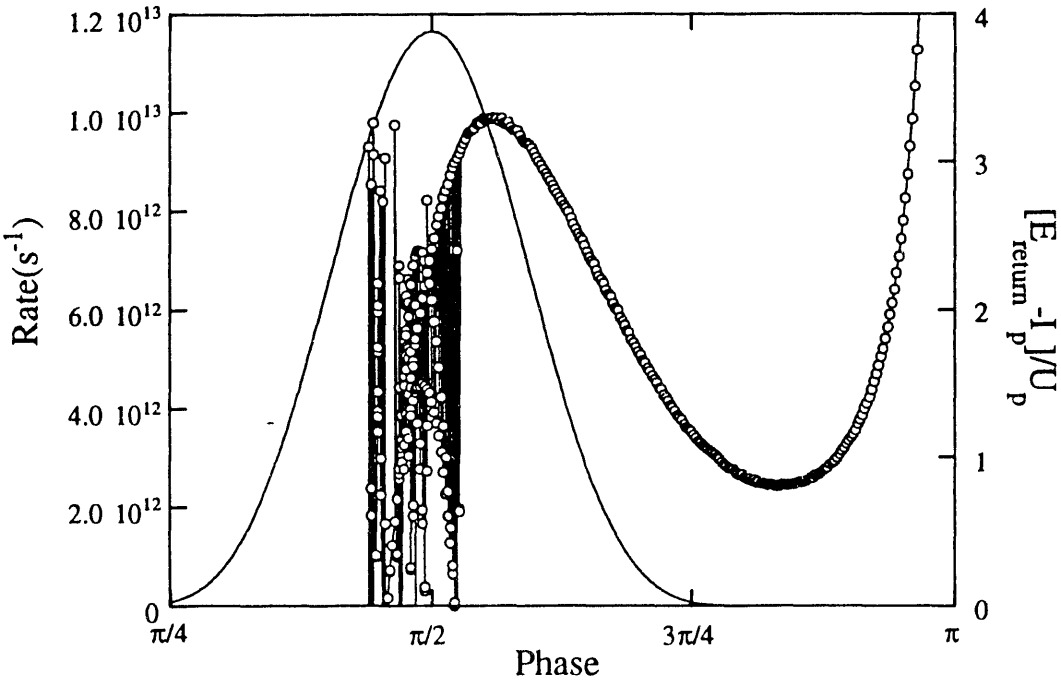

Fig. 7 Hydrogen tunnelling rate (solid line-left axis) and energies of returning trajectories at the nucleus (symbols-right axis) as a functions of the phase of the oscillating field ($I = 10^{14}$ W/cm^2).

In Fig. 8 we show a histogram of the return energies weighted by the tunnelling rate appropriate to the initial conditions for each trajectory. The result is a broad, flat distribution out to approximately $3.2U_p$ followed by an abrupt cutoff. One can see from Fig. 7 that return energies much above the cutoff are possible for phases near π, but these again are the result of initial displacements which are very large and therefore due to such thick barriers that the tunnelling rate is negligible. For probable initial conditions, the return energies do

not exceed $I_p + 3.2U_p$. *We believe this energy distribution provides the source for the plateau in the harmonic spectrum.* As each trajectory returns to the nucleus, it will have a probability for emitting a photon which is proportional to the oscillator strength of transition back to the ground state at the return energy. The optical field is varying so slowly during the high energy collision that one can reasonably approximate the transition strength by its field-free value. For hydrogen at these energies, the oscillator strength[18] is decreasing by approximately ω^{-3}. Weighting the probabilities in Fig. 8 by this factor we obtain this second contribution to the high-order harmonic spectrum which is shown in Fig. 4b. In the lowest portion of this figure we have combined, again schematically, the two components of the spectrum. We have assumed the harmonics in the plateau scale approximately as the fifth power of the incident intensity and those from the short-range "perturbative" effects of the anharmonic, atomic potential according to their individual power laws. Although the real atomic spectrum is the result of a coherent sum of the contributions from these different sources, the figure does illustrate the relative strengths and distributions from the two processes which are involved.

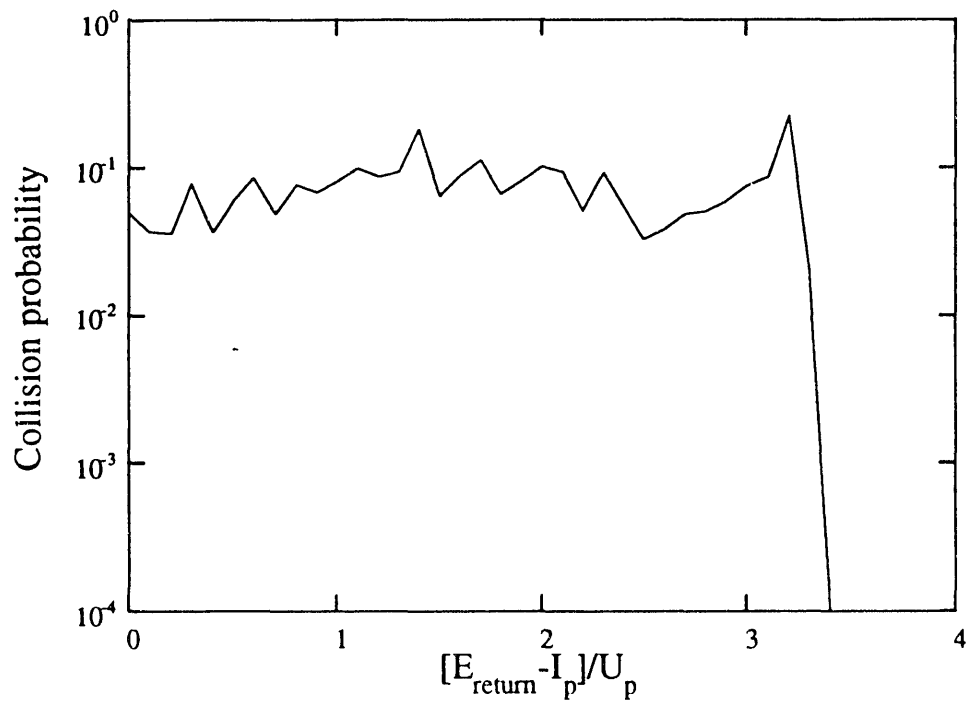

Fig. 8 Energy histogram for electron trajectories returning to the nucleus for hydrogenic, soft-Coulomb potential: $\hbar\omega = 0.025$ au and $I = 1\times10^{14}$ W/cm^2.

The harmonic plateau has a distinct cutoff because the field can transfer a limited amount of energy to the electron before it returns to the nucleus. Because of this the harmonics beyond the plateau, coming only from the short-range distortion of the charge density, should behave perturbatively. Although it is beyond the scope of this contribution to

consider the phase matching effects on the harmonic signals, we should mention that the angular distributions of the harmonics depend on the effective order, p, of the single-atom signal.[4,15] In the example shown in Fig. 4b we assumed the effective order was 5 which is representative of what we find in our calculations. This says, for example that the 41st harmonic, if it is within the plateau, scales with incident intensity as I^5 rather than the I^{41} one would expect from a perturbative response. The width of the angular distribution scales roughly as $p^{-1/2}$ which means the spatial distribution of the plateau harmonics should be *much* broader than for those beyond the cutoff. In a separate contribution to this meeting the group from Imperial College[19] showed that the angular distributions of harmonics generated in helium exhibited this expected dramatic narrowing as the cutoff in the plateau is approached. This picture of two distinct sources for high-order harmonics is also reinforced by the observed intensity dependences of the individual harmonics. Both the Stanford group[3a] and the Saclay/Lund collaboration[20] have observed that the harmonics initially rise very rapidly as the intensity increases then flatten out very abruptly as they join the plateau. In this narrow transition region the source of the harmonics is changing from the short-range dynamics to that governed by the acceleration of the electron far from the atom by the oscillating field.

Finally we wish to consider the consequences of this picture of two-step ionization dynamics on the other emission process occurring at the same time as harmonic generation. This is the production of very high energy electrons (ATI). If we compare the xenon results presented above for photon and electron emission rates we can see that there is a distinct difference in that the cutoff in the harmonic spectrum is not present in the ATI. In Fig. 9 we compare the single-atom emission strengths for the two processes at four different intensities. The harmonic emission strength is given by ω^3 times $|d_q|^2$. We have also noted in this figure the predicted cutoffs, $I_p + 3U_p$, for the harmonics. As discussed above, without additional collisions with the nucleus the electrons would not have energies larger than $3U_p$, but they clearly do. Also by examining Fig. 7 we see that the electrons released near the maximum of the field during the cycle, which will have the lowest initial drift velocity, are those responsible for the highest harmonic photons. Therefore, this model shows there is not a simple, direct connection between the ATI and harmonic spectra. That is, the portion of the wave function responsible for highest energy photons does not necessarily correspond to that which ends up in the ATI peaks of the same order. However below the harmonic cutoff the harmonic and ATI strengths are clearly very similar. The reason the overall strengths scale similarly with intensity is that these are governed by the initiation step which is the rate at which electrons are released to the continuum. This quantum mechanical first step, tunnelling through the barrier, defines the number of electrons available to either produce photons or be measured in the ATI spectrum. It is this aspect of the ionization process which depends sensitively on the details of the atomic potential. The subsequent evolution of the electrons in the continuum should be essentially the same for all systems, depending only on

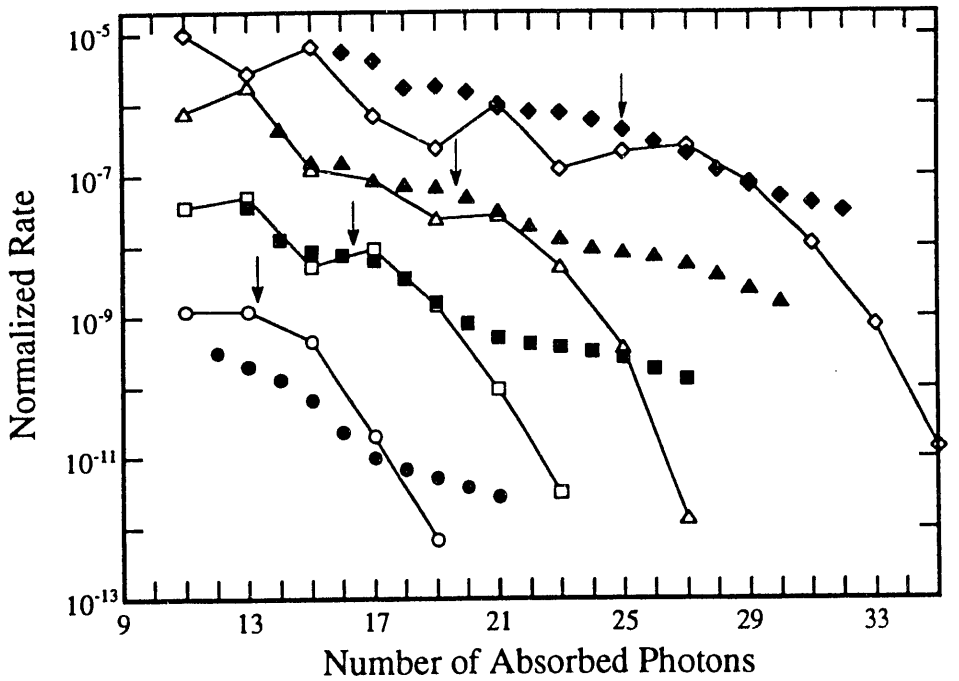

Fig. 9 Photon (open symbols) and electron (filled symbols) emission rates for xenon at 1.06 μm and intensities of 1 (circles), 2 (squares), 3 (triangles) and 5 (diamonds) x10^{14} W/cm^2. The harmonic rates have been scaled to agree with the electron rate for the 21st order peaks for the highest intensity shown.

the ionization potential and the ponderomotive energy. This explains our earlier observations[11,21] of virtually identical plateau distributions for several model potentials all of which were constructed to have the same I_p. The models included the hydrogen atom and molecule, a short range potential which had no excited states and a one-dimensional soft-Coulomb potential. The overall strengths of the calculated plateaus for these systems were quite different, reflecting the different rates at which electrons were promoted to the continuum, but the shape of the spectrum was very similar with the cutoff in all cases being accurately predicted by $I_p + 3U_p$. The harmonic spectrum probes the distribution of velocities near the nucleus while the electron spectrum measures the distribution of drift velocities after the electrons have completely escaped from the effects of the potential. One signature of this difference is that the additional collisions necessary for the higher energy electrons should lead to increasing angular distributions of the ATI peaks. In Fig.10 we show calculated[2] halfwidths of the angular distributions for hydrogen ATI peaks which do show minima near $3U_p$ followed by increasing breadth for higher orders. These results agree well with the observations of Wolff et al.[22] for the same conditions.

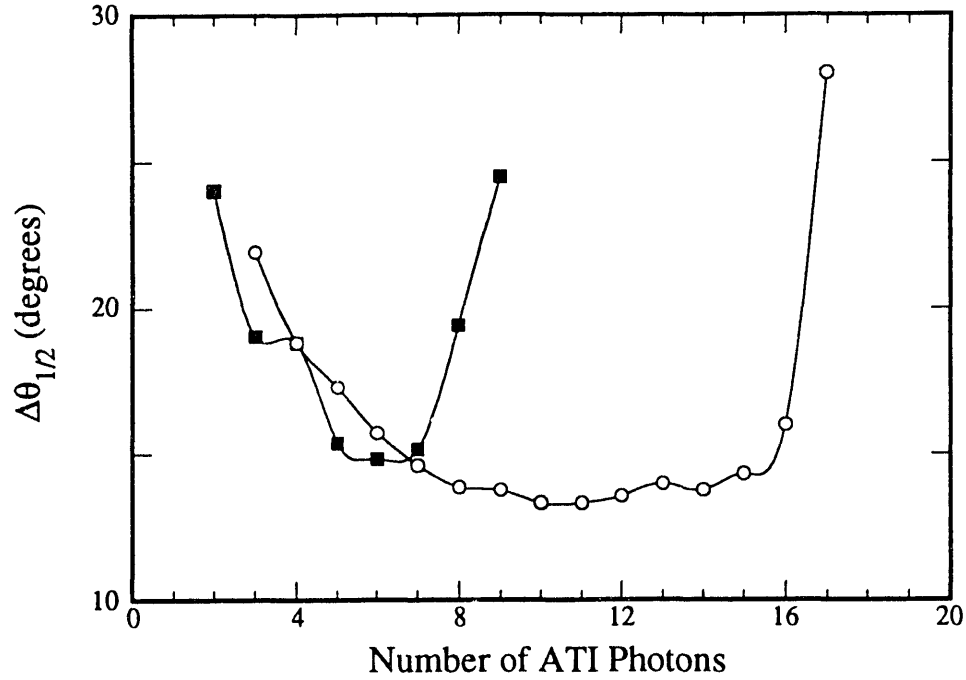

Fig. 10 Half heights of ATI peaks calculated for hydrogen at 2 (squares) and 3 (circles) x10^{13} W/cm^2 and a wavelength of 1.06 μm.

The calculations we have presented in this paper illustrate the application of our single-active-electron model of intense-field, multiphoton processes. We have found that it is very successful in modelling very high order, non-perturbative processes in rare gas atoms. The simple two-step, quasi-classical model which accounts for many of the detailed characteristics of the phōton and electron emission processes provides significant new insight into the excitation dynamics under intense field conditions.[23]

ACKNOWLEDGEMENT

We wish to acknowledge the very significant contributions to this work by our collaborators Anne L'Huillier and Phillipe Balcou from Saclay for the results presented on harmonics and Louis Franklin DiMauro and Baorui Yang from Brookhaven for the ATI results. This work has been carried out under the auspices of the U. S. Department of Energy at the Lawrence Livermore National Laboratory under contract number W-7405-ENG-48.

REFERENCES

* Present address: Department of Chemistry, University of California at San Diego

1. G. Petit, P. Agostini and F. Yergeau, J. Opt. Soc. Am. B 4:765 (1987).
2. K. J. Schafer and K. C. Kulander, Phys. Rev. A 42:5794 (1990); K. J. Schafer, Comp. Phys. Comm. 63:427 (1991).
3. (a) J. Macklin, J. D. Kmetec and C. L. Gordon III, Phys. Rev. Lett. 70:766 (1993); (b) A. L'Huillier and P. Balcou, Phys. Rev. Lett. 70:774 (1993).
4. A. L'Huillier, K. J. Schafer and K. C. Kulander, J. Phys. B 24:3315 (1991).
5. K. C. Kulander, K. J. Schafer and J. L. Krause, Time-dependent studies of multiphoton processes, in: "Atoms in Intense Radiation Fields," M. Gavrila, ed. (Advances in Atomic, Molecular and Optical Physics, Supplement 1) Academic Press, New York (1992)
6. K. C. Kulander and T. N. Rescigno, Comp. Phys. Comm. 63:523 (1991).
7. K. C. Kulander, J. L. Krause, K. J. Schafer, S. W. Allendorf, J. K. Crane, K. S. Budil and M. D. Perry, in Time Dependent Quantum Molecular Dynamics: Experiment and Theory, J. Broekhove and L. Lathouwers, Eds. (Plenum, New York, 1992).
8. S. W. Allendorf, J. K. Crane, K. S. Budil and M. D. Perry, to be published.
9. K. C. Kulander, Phys. Rev. A 38:778 (1988).
10. K. C. Kulander and B. W. Shore, J. Opt. Soc. B 7:502 (1990).
11. J. L. Krause, K. J. Schafer and K. C. Kulander, Phys. Rev. A 45:4998 (1992).
12. K. Burnett, V. C. Reed, J. Cooper and P. L. Knight, Phys. Rev. A 45:3347 (1992).
13. K. J. Schafer, B. Yang, L. F. DiMauro and K. C. Kulander, Phys. Rev. Lett. 70:xxxx (1993).
14. A. L'Huillier, P. Balcou, C. Candel, K. J. Schafer and K. C. Kulander, Phys. Rev. A 46:2778 (1992).
15. B. W. Shore and K. C. Kulander, J. Mod. Opt. 36:857 (1989).
16. P. B. Corkum, N. H. Burnett and F. Brunel, Phys. Rev. Lett. 62:1259 (1989).
17. J. Javanainen, Q. Su and J. H. Eberly, Phys. Rev. A 38:3430 (1988). The parameter in the denominator of this potential is set to 2.0 to obtain a binding energy of 13.6 eV.
18. H. A. Bethe and E. E. Salpeter. "Quantum Mechanics of One- and Two-Electron Atoms," Plenum, New York (1977).
19. R. A. Smith, J. W. G. Tisch, M. S. N. Ciarrocca, S. Augst and M. H. R. Hutchinson, this workshop.
20. J. Larsson, A. Persson, S.Svanberg, C.-G. Wahlström, P. Balcou and A. L'Huillier, this workshop.
21. J. L. Krause, K. J. Schafer and K. C. Kulander, Phys. Rev. Lett. 68:3535 (1992).
22. B. Wolff, H. Rottke, D. Feldmann and K. H. Welge, Z. Phys. D 10:35 (1988).
23. We note that Paul Corkum has independently extended his quasi-static model (Ref. 16) also along these lines to consider both harmonic generation and impact ionization of the ion core by returning electrons.

DATE
FILMED
9/10/93

END